Generation of a radially polarized light beam using internal conical diffraction

C. F. Phelan,[1] J. F. Donegan,[1,2,*] and J. G. Lunney[1,2]

[1]*School of Physics, Trinity College Dublin, Dublin 2, Ireland*
[2]*CRANN Research Institute, Trinity College Dublin, Dublin 2, Ireland*
*jdonegan@tcd.ie

Abstract: Using a combination of internal conical diffraction and Mach-Zehnder interferometry we have theoretically and experimentally demonstrated an efficient new technique for the conversion of a linearly polarized Gaussian laser beam to one with radial polarization. These methods that can be adapted to yield either ring-shaped or first order Bessel beams which are radially polarized.

OCIS codes: (260.1180) Crystal optics; (140.3300) Laser beam shaping; (260.5430) Polarization

References and links

1. K. S. Youngworth and T. G. Brown, "Focusing of high numerical aperture cylindrical-vector beams," Opt. Express **7**(2), 77–87 (2000).
2. Y. Saito, M. Kobayashi, D. Hiraga, K. Fujita, S. Kawano, N. I. Smith, Y. Inouye, and S. Kawata, "Z-polarization sensitive detection in micro-Raman spectroscopy by radially polarized incident light," J. Raman Spectrosc. **39**(11), 1643–1648 (2008).
3. S. Quabis, R. Dorn, M. Eberler, O. Glokl, and G. Leuchs, "Focusing light to a tighter spot," Opt. Commun. **179**(1-6), 1–7 (2000).
4. S. C. Tidwell, D. H. Ford, and W. D. Kimura, "Generating radially polarized beams interferometrically," Appl. Opt. **29**(15), 2234–2239 (1990).
5. Y. Kozawa and S. Sato, "Generation of a radially polarized laser beam by use of a conical Brewster prism," Opt. Lett. **30**(22), 3063–3065 (2005).
6. W. J. Lai, B. C. Lim, P. B. Phua, K. S. Tiaw, H. H. Teo, and M. H. Hong, "Generation of radially polarized beam with a segmented spiral varying retarder," Opt. Express **16**(20), 15694–15699 (2008).
7. G. Machavariani, Y. Lumer, I. Moshe, A. Meir, and S. Jackel, "Efficient extracavity generation of radially and azimuthally polarized beams," Opt. Lett. **32**(11), 1468–1470 (2007).
8. Y. Tokizane, K. Shimatake, Y. Toda, K. Oka, M. Tsubota, S. Tanda, and R. Morita, "Global evaluation of closed-loop electron dynamics in quasi-one-dimensional conductors using polarization vortices," Opt. Express **17**(26), 24198–24207 (2009).
9. M. V. Berry, "Conical diffraction asymptotics: fine structure of Poggendorff rings and axial spike," J. Opt. A, Pure Appl. Opt. **6**(4), 289–300 (2004).
10. A. M. Belsky and A. P. Khapaluyk, "Internal conical refraction of bounded light beams in biaxial crystals," Opt. Spectrosc. **44**, 312–315 (1978).
11. W. R. Hamilton, "Third supplement to an essay on the theory of systems of rays," Trans. R. Irish Acad. **17**, 1–144 (1837).
12. H. Lloyd, "On the phenomena presented by light in its passage along the axes of biaxial crystals," Phil. Mag. **1**, 112–120 (1833).
13. H. Lloyd, "On the phenomena presented by light in its passage along the axes of biaxial crystals," Phil. Mag. **1** 207–210 (1833).
14. L. D. Landau, E. M. Lifshitz, and L. P. Pitaevskii, *Electrodynamics of Continuous Media,* 2nd ed. (Pergamon, 1984).
15. C. F. Phelan, D. P. O'Dwyer, Y. P. Rakovich, J. F. Donegan, and J. G. Lunney, "Conical diffraction and Bessel beam formation with a high optical quality biaxial crystal," Opt. Express **17**(15), 12891–12899 (2009).
16. V. Peet, "Biaxial crystal as a versatile mode converter," J. Opt. **12**(9), 095706 (2010).
17. D. P. O'Dwyer, C. F. Phelan, K. E. Ballantine, Y. P. Rakovich, J. G. Lunney, and J. F. Donegan, "Conical diffraction of linearly polarised light controls the angular position of a microscopic object," Opt. Express **18**(26), 27319–27326 (2010).
18. M. C. Pujol, M. Rico, C. Zaldo, R. Solé, V. Nikolov, X. Solans, M. Aguiló, and F. Díaz, "Crystalline structure and optical spectroscopy of Er^{3+}-doped $KGd(WO_4)_2$ single crystals," Appl. Phys. B **68**(2), 187–197 (1999).
19. M. V. Berry, M. R. Jeffrey, and M. Mansuripur, "Orbital and spin angular momentum in conical diffraction," J. Opt. A, Pure Appl. Opt. **7**(11), 685–690 (2005).

#152718 - $15.00 USD Received 10 Aug 2011; revised 21 Sep 2011; accepted 21 Sep 2011; published 20 Oct 2011

1. Introduction

Radially and azimuthally polarized light beams fall within the class of cylindrically symmetric vector beams whose polarization vectors are oriented in the radial and azimuthal directions respectively; it is assumed that the radius vector is drawn from the centre of the beam as shown in Fig. 1. Since a radially polarized light beam can be converted to an azimuthally polarized beam by propagation through two half-wave plates with an angle of 45° between their fast axes, this paper will only consider radial polarization and how it can be produced using conical diffraction.

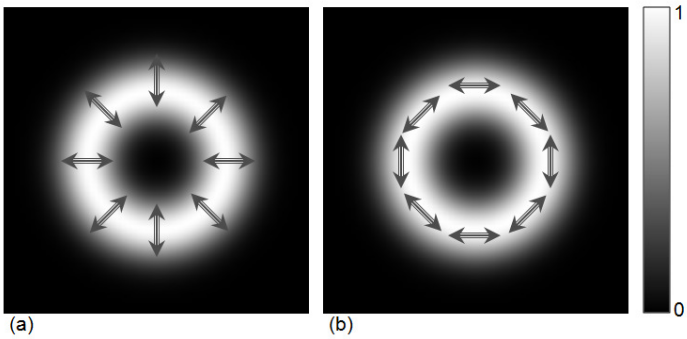

Fig. 1. Transverse distribution of intensity and polarization (arrows) in (a) radially polarized and (b) azimuthally polarized light beams.

When a radially polarized beam is tightly focused the electric field can have a relatively large longitudinal component due to destructive interference of the transverse components [1]. This property forms the basis of z-polarization spectroscopy [2]. A radially polarized beam can be focused to a smaller spot than can be achieved with a comparable beam with linear or circular polarization [3]. There are several techniques available for the generation of radially polarized beams, such as optical interference [4] and propagation through a conical Brewster prism [5] or segmented spiral phase plate [6, 7]. Jones matrices for a system that transform a circularly or linearly polarized beam into a radially polarized beam are given in Refs [4, 8].

of In this paper, the results of some experiments to demonstrate the conversion of the polarization of a Gaussian beam from linear to radial using internal conical diffraction (ICD) are described. Conical diffraction [9, 10] refers to the paraxial wave theory extension of the geometrical optics treatment of conical refraction [11–14]. ICD arises when a narrow light beam is directed along one of the optic axes of a biaxial crystal; it propagates as a hollow cone of light within the crystal and emerges as a hollow cylinder of radius R_0, as shown in Fig. 2. In ICD a weakly focussed Gaussian beam is transformed to a double ring-shaped beam (Fig. 2(b)) where the aspect ratio of the rings depend on the ratio $\rho_0 = R_0/\omega_0$, where ω_0 is the beam waist radius of the incident beam. The predictions of paraxial ICD theory have been shown to agree well with experiment [15]. Recently, Peet [16] has exploited this dependence of the shape the ICD beam on incident beam waist to develop an efficient technique for the conversion of a Gaussian beam to either a Hermite-Gaussian or Laguerre-Gaussian beam profile. In the work reported here the unusual polarization properties of the ICD beam are exploited to yield a novel and efficient method of generating a radially polarized beam. In addition, the shape of the radially polarized beam can be varied by changing the ω_0:R_0 ratio.

#152718 - $15.00 USD Received 10 Aug 2011; revised 21 Sep 2011; accepted 21 Sep 2011; published 20 Oct 2011

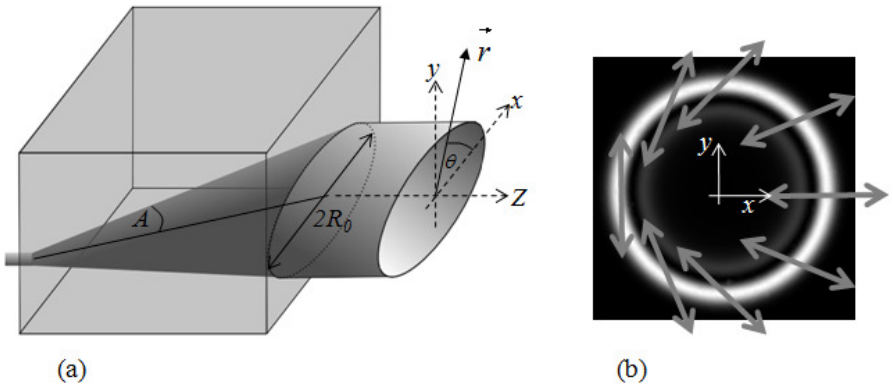

Fig. 2. (a) Schematic diagram showing the geometry of internal conical diffraction. (b) The FIP intensity and polarization distribution for a conically diffracted Gaussian beam where ω_0:R_0 = 1:9.

2. Theory

The transformation of a Gaussian laser beam by ICD in a biaxial crystal of length l, with principal refractive indices $n_1<n_2<n_3$ and with its entrance and exit faces cut perpendicular to one of its optic axes is described in Ref [7]. For a beam with an electric field profile at the beam waist of the form: $\exp[-r^2/\omega_0^2]$ the spatial Fourier transform has the form: $\sqrt{\pi\omega_0^2}\exp[-\omega_0^2 k^2 P^2/4]$, where $k\vec{P}$ is the transverse component of the wave-vector in the crystal with $k = n_2 k_0$ where k_0 is the vacuum wave number. If the polarization of the beam incident on the biaxial crystal is described by the Jones vector $\{e_x, e_y\}$, the ICD beam is a superposition of two components and is described by:

$$\vec{E}(r,\theta,Z) = \mathrm{B}_0(r,Z)\begin{pmatrix} e_x \\ e_y \end{pmatrix} + \mathrm{B}_1(r,Z)\begin{pmatrix} \cos\theta & \sin\theta \\ \sin\theta & -\cos\theta \end{pmatrix}\begin{pmatrix} e_x \\ e_y \end{pmatrix}, \tag{1}$$

$$\mathrm{B}_0(r,Z) = \sqrt{\pi k^2\omega_0^2}\int_0^\infty P e^{-\frac{1}{2}ikP^2 Z}\cos(kPR_0)J_0(rkP)e^{-\frac{1}{4}\omega_0^2 k^2 P^2}\,dP, \tag{2}$$

$$\mathrm{B}_1(r,Z) = \sqrt{\pi k^2\omega_0^2}\int_0^\infty P e^{-\frac{1}{2}ikP^2 Z}\sin(kPR_0)J_1(rkP)e^{-\frac{1}{4}\omega_0^2 k^2 P^2}\,dP. \tag{3}$$

The co-ordinates $\{r,\theta,Z\}$ used in these equations are shown in Fig. 2 and J_n refers to the n^{th} order Bessel function of the first kind. The co-ordinate Z is defined as: $Z = l + (z-l)n_2$, where n_2 is the intermediate principal refractive index of the crystal and z is measured from beam waist in the absence of the biaxial crystal. The radius of the ring-shaped beam is given by: $R_0 = Al$, where A is the cone angle (Fig. 2) given by $A = \sqrt{(n_2-n_1)(n_3-n_2)}$ and l is the length of the crystal. In ICD the ring-shaped beam is most sharply defined at the position Z = 0 which is called the focal image plane (FIP) and corresponds to the image of the beam waist in the crystal [7, 15]. Figure 2(b) shows a calculation of the FIP intensity profile calculated for a circularly polarized input beam where ρ_0 = 9. The intensity in the ICD beam is azimuthally uniform and linearly polarized at each point such that the plane of polarization rotates by 180° on making a circuit of the beam propagation axis (z). When the Gaussian waist ω_0 is small compared to the ring radius R_0 the far-field distributions (at large Z) of the two beam components B_0 and B_1 are closely approximated by zeroth and first order Bessel functions, respectively. If the input beam is linearly polarized the output beam is crescent-shaped with

#152718 - $15.00 USD Received 10 Aug 2011; revised 21 Sep 2011; accepted 21 Sep 2011; published 20 Oct 2011

an intensity maximum at the azimuthal position where the polarization with a circularly polarized input corresponds to the plane of polarization of the incident beam, as shown in Fig. 3(b) for horizontally polarized input. This crescent shaped beam has recently been used as the basis for a novel type of optical trap [17]. If, as shown in Fig. 3(c), the crescent-shaped beam is propagated through a second linear polarizer oriented orthogonal to the input polarization the region of maximum intensity is not transmitted and the crescent-shaped beam is transformed into a double lune-shaped beam which bears some resemblance to a Hermite-Bessel beam. The line of zero intensity is parallel to the input polarization.

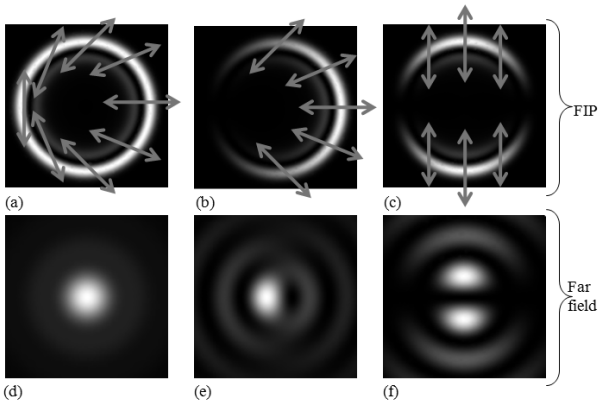

Fig. 3. The FIP intensity distribution for conical diffraction of Gaussian beams: (a) circularly polarized, (b) linearly (horizontal) polarized Gaussian beams and (c) when the (b) propagates through a vertically aligned linear polarizer. (d), (e) and (f) show the far field profiles corresponding to (a), (b) and (c) respectively.

If the FIP intensity distributions shown in Fig. 3(a), 3(b) and 3(c) are allowed to propagate well beyond the Rayleigh range, the respective far-field beams shown in Fig. 3(d), 3(e) and 3(f) are formed.

The unusual intensity and polarization profiles shown in Fig. 3 can be exploited in two distinct methods to generate a radially polarized beam, as illustrated in Fig. 4. In the first method, the radially polarized beam is formed by coherent superposition of two Hermite-Bessel-like beams with one rotated by 90°, as shown in Fig. 4(a) for FIP and in Fig. 4(b) for the far-field.

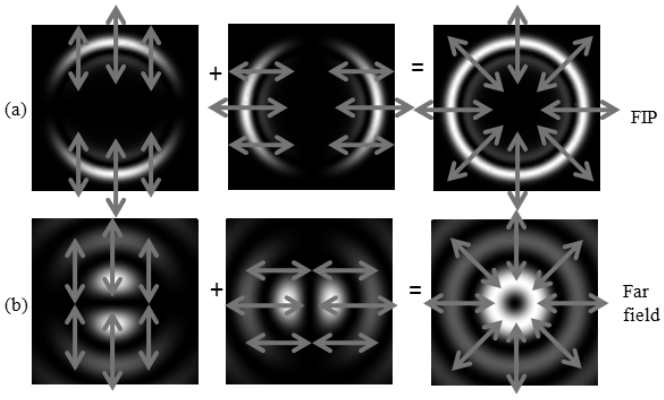

Fig. 4. Schematic diagram showing the formation of radially polarized beams by superposition of equal amplitude orthogonal Hermite-Bessel-like beams in (a) the FIP and (b) the far field.

#152718 - $15.00 USD Received 10 Aug 2011; revised 21 Sep 2011; accepted 21 Sep 2011; published 20 Oct 2011

The second method uses superposition of a crescent-shaped beam with its mirror image, as shown in Fig. 5.

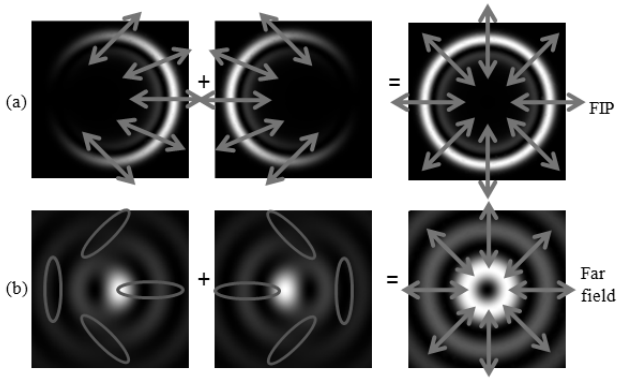

Fig. 5. Schematic diagram showing the formation of radially polarized beams by the superposition of a crescent-shaped beam with its mirror image in (a) the FIP and (b) the far field. The ellipses in (b) indicate elliptical polarization.

3. Experiment

Both of the methods of generating radial polarization illustrated in Figs. 4 and 5 were demonstrated using a Mach Zehnder interferometer for coherent beam superposition. In the first instance it was easier to record the images of the radially polarized beam in the far field and hence the intensity distributions resemble that of a first order Bessel beam. Later, it is shown that the FIP distributions can be recovered.

The basic optical arrangement used to generate the radially polarized beams is shown in Fig. 6. The light source was a 10 mW He-Ne laser operating at 632 nm with a Gaussian beam output. The beam entering the crystal was linearly polarized and focused with a 10 cm focal length lens to a beam waist radius of 60 μm. The beam waist was formed beyond the crystal at ~11 cm from the lens; this is the location of the FIP mentioned above. The biaxial crystal used in this experiment was a 20.9 mm long slab of $KGd(WO_4)_2$ with refractive indices n_1 = 2.013, n_2 = 2.045, n_3 = 2.086 [18] leading to an R_0 value of 0.37 mm. The Mach-Zehnder interferometer was constructed as shown in Fig. 6. Neutral density filters (NDF) were used to equalise the beam amplitudes in the two arms and a Dove prism was placed in Arm 2 to rotate the beam in that arm by 90° or 180° as required. A Dove prism is a truncated right angle prism (Fig. 6). A beam that enters the prism is inverted by total internal reflection off the prism base (longest surface) about an axis of inversion parallel to the edge between the base and entrance face (orthogonal to the page in Fig. 6). By rotating the prism about the optic axis we are rotating this axis of inversion about the optic axis. Thus if we initially locate the base of the Dove prism in the x, z plane the image will be inverted about the x axis. Rotating the prism will rotate this inverted image by twice the angle the prism is rotated by. The change of handedness caused by propagation through the Dove prism did not affect our method. Mirror 2 was mounted on a piezoelectric drive to accurately adjust the phase difference between the two beams.

#152718 - $15.00 USD Received 10 Aug 2011; revised 21 Sep 2011; accepted 21 Sep 2011; published 20 Oct 2011

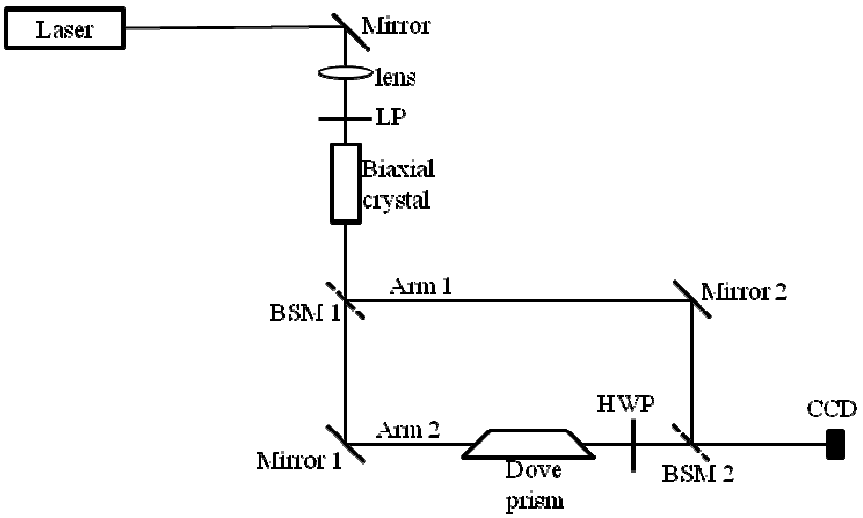

Fig. 6. The basic experimental setup used to convert a linearly polarized Gaussian to a radially polarized beam using conical diffraction and an interferometer. LP is a linear polarizer, BSM is a beam-splitter, HWP is a half wave-plate and CCD is a charge-coupled device camera.

Method 1

The first method of generating a radially polarized beam using ICD involves the coherent superimposition of two Hermite-Bessel-like beams with one rotated by 90°. The Hermite-Bessel beam was prepared by sending a Gaussian beam linearly polarized in the horizontal (x) direction through a biaxial crystal followed by a linear polarizer (not shown in Fig. 6) with the transmission in the orthogonal direction. The beam incident on the first beam splitter (BSM 1) is obtained from Eq. (1) by setting the incident polarization vector as $\begin{pmatrix} 1 \\ 0 \end{pmatrix}$ and then applying the Jones matrix for the linear polarizer $\begin{pmatrix} 0 & 0 \\ 0 & 1 \end{pmatrix}$. The result is:

$$\mathrm{B}_1 \sin\theta \begin{pmatrix} 0 \\ 1 \end{pmatrix}, \tag{4}$$

The polarization and intensity distribution associated with this beam are depicted in Fig. 3(c) and Fig. 3(f) in the near and far field respectively. In order to rotate the polarization and intensity profile of this beam by 90° about the optic axis the beam propagates through a Dove prism followed by a HWP. The axis of inversion of the Dove prism made a 45° angle with the horizontal (as well as vertical). The fast axis of the HWP was also set at 45° to the horizontal so as to rotate the polarization by 90°. Figure 7(a) shows the beam in Arm 1 (recorded by blocking Arm 2) and Fig. 7(b) shows the beam in Arm 2 after the Dove prism and HWP. The form of the beam that emerges from Arm 2 is obtained from Eq. (4) by making the substitution $\theta \to -\theta + 90^{\circ}$ representing the effect of the Dove prism (which inverts as well as rotates the image) and then applying the Jones matrix $\begin{pmatrix} 0 & 1 \\ 1 & 0 \end{pmatrix}$ for the HWP described above. After recombination at BSM 2 the output beam has the form:

$$\mathrm{B}_1 \sin\theta \begin{pmatrix} 0 \\ 1 \end{pmatrix} - e^{i\delta}\, \mathrm{B}_1 \cos\theta \begin{pmatrix} 1 \\ 0 \end{pmatrix}, \tag{5}$$

#152718 - $15.00 USD Received 10 Aug 2011; revised 21 Sep 2011; accepted 21 Sep 2011; published 20 Oct 2011

where δ is the phase difference between the beams. When $\delta = \pi$ the output beam is radially polarized and described by:

$$B_1 \begin{pmatrix} \cos\theta \\ \sin\theta \end{pmatrix}. \tag{6}$$

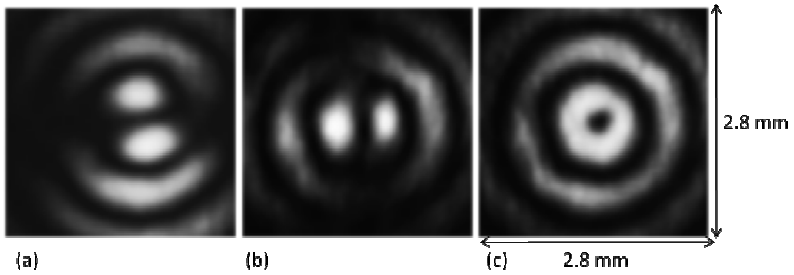

Fig. 7. Intensity distributions of (a) the beam from Arm 1 on its own, (b) the beam from Arm 2 on its own, and (c) the superposition beam.

The radial polarization of the beam in Fig. 7(c) was confirmed by recording the intensity distribution as a linear polarizer is rotated in the beam, as shown in Fig. 8. As expected the intensity distribution is bisected by a line of zero intensity oriented orthogonal to the transmission axis of the polarizer.

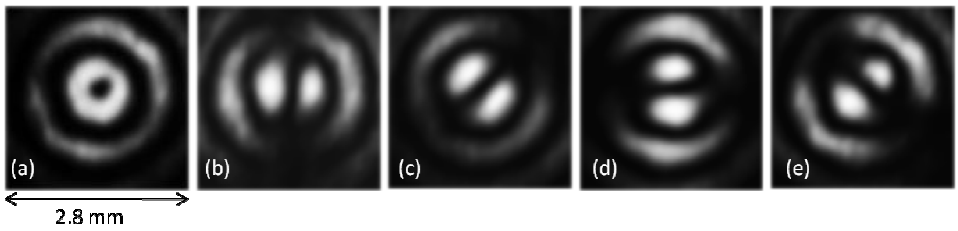

Fig. 8. Intensity profiles recorded when the radially polarized beam of method 1 (a) is transmitted through a linear polarizer with the transmission axis set at follows: (b) horizontal, (c) at 45° to horizontal, (d) vertical and (e) 135° to horizontal.

Method 2

In the second method of generating a radially polarized beam the crescent-shaped beam shown in Fig. 3(b) is coherently superimposed with is mirror image. The input beam is linearly polarized making the output beam crescent-shaped as described above and polarized as shown in Fig. 3(b). Thus the crescent beam entering the interferometer and propagating in Arm 1 is described by:

$$B_0 \begin{pmatrix} 1 \\ 0 \end{pmatrix} + B_1 \begin{pmatrix} \cos\theta \\ \sin\theta \end{pmatrix}. \tag{7}$$

In Arm 2 the mirror image of this beam is formed by propagation through the Dove prism with the base (longest surface) of the prism located the {y, z} plane and the axis of inversion along the y axis. Thus the image of the beam is inverted about the y axis. Of course, the Dove prism does not rotate the polarizations as is required, rather, this is done by the HWP in Arm 2 which is set with the fast axis parallel to plane of polarization of the input beam (along the x direction). The beam emerging from Arm 2 is obtained from Eq. (7) by setting $\theta \to 180^{o} - \theta$ and applying the Jones matrix for the HWP $\begin{pmatrix} 1 & 0 \\ 0 & -1 \end{pmatrix}$. The result is:

#152718 - $15.00 USD Received 10 Aug 2011; revised 21 Sep 2011; accepted 21 Sep 2011; published 20 Oct 2011

$$B_0\begin{pmatrix}1\\0\end{pmatrix}-B_1\begin{pmatrix}\cos\theta\\\sin\theta\end{pmatrix}. \tag{8}$$

The superposition beam is given by:

$$B_0\begin{pmatrix}1\\0\end{pmatrix}+B_1\begin{pmatrix}\cos\theta\\\sin\theta\end{pmatrix}+e^{i\delta}\left\{B_0\begin{pmatrix}1\\0\end{pmatrix}-B_1\begin{pmatrix}\cos\theta\\\sin\theta\end{pmatrix}\right\}, \tag{9}$$

where δ is the phase difference. Both the FIP and far-field intensity distributions depend on value of δ. Figure 9 shows the far-field distributions, calculated according to Eq. (9), for δ = 0, π/2 and π. For δ = 0 the B_1 terms in Eq. (9) cancel and the superposition beam is linearly polarized and J_0-like in character. For δ = π the B_0 terms cancel and a radially polarized J_1-like beam is formed. Thus, it is possible to switch between a radially polarized beam J_1-like and a linearly polarized J_0-like beam by varying δ. For intermediate cases the beam is a mixture of B_0 and B_1 components. If δ is set at π/2 the B_0 and B_1 terms in Eq. (9) have the same coefficients and we have a standard conically diffracted Gaussian intensity distribution (Fig. 9(b)).

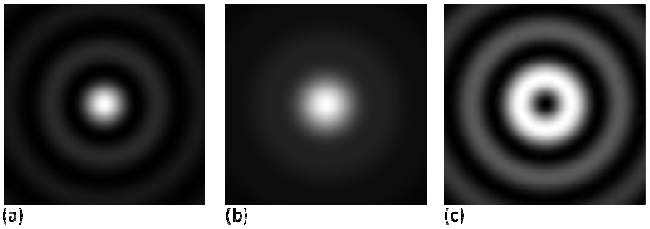

Fig. 9. Far-field intensity profiles predicted by Eq. (9) for (a) δ = 0; (b) δ = π/2 and (c) δ = π, which yields the radially polarized beam

Figure 10(a) shows an image of the intensity distribution of the superposition beam obtained with the interferometer adjusted to yield the radially polarized beam. Figure 10(b) shows a comparison of the measured and calculated radial intensity distributions, which, of course, are close to the B_1 Bessel profile at this location. The fact that we have a B_1 profile implies, from the above considerations, that the beam is radially polarized. As before, the radial polarization was confirmed by rotating a linear polarizer in the beam as is shown in Fig. 11.

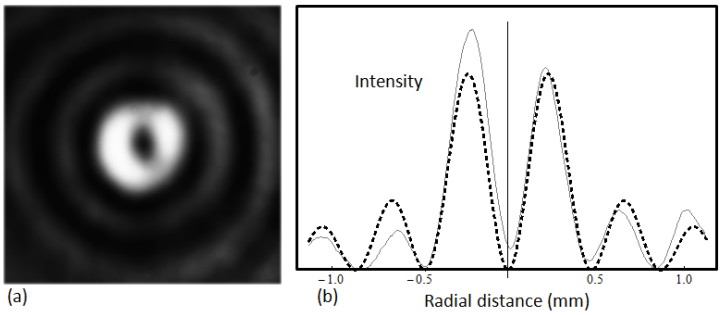

Fig. 10. (a) CCD image of the radially polarized beam formed by the superposition of crescent beams. (b) Comparison of the measured (solid line) and calculated (dashed line) radial intensity profiles.

#152718 - $15.00 USD Received 10 Aug 2011; revised 21 Sep 2011; accepted 21 Sep 2011; published 20 Oct 2011

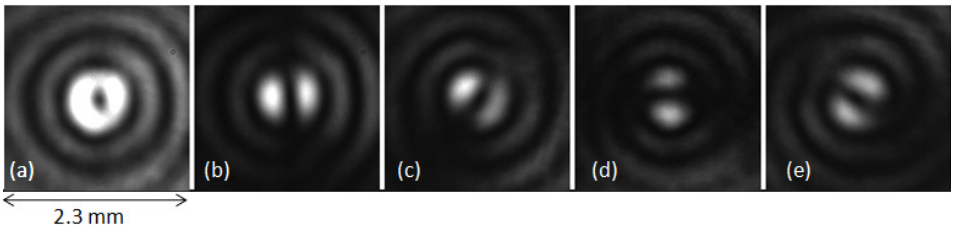

Fig. 11. Intensity profiles recorded when the radially polarized beam of method 2 (a) is transmitted through a linear polarizer with the transmission axis set at follows: (b) horizontal, (c) at 45° to horizontal, (d) vertical and (e) 135° to horizontal.

As mentioned earlier, the ICD of a Gaussian beam yields a beam which has double ring profile in the near-field (close to the FIP) which diffracts to a Bessel-like intensity distribution in the far field. For the optical system in Fig. 6 the CCD camera is positioned in the far-field of the conically diffracted beam. However, it is possible to recover the FIP profiles by using the simple imaging system as shown in Fig. 12 to relay the FIP to the detector plane.

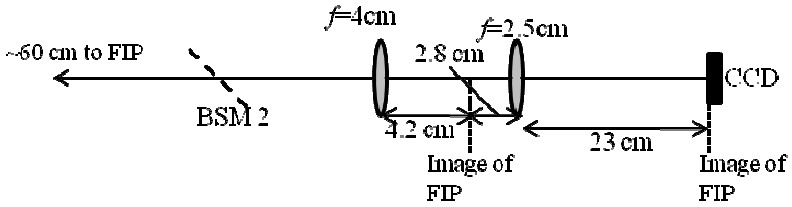

Fig. 12. The optical system used to relay the FIP to the detector plane.

Figure 13 shows the FIP intensity distributions of the two crescent-shaped beams and the radially polarized superposition beam obtained in using the first method of synthesising a radially polarized beam. As expected the double-ring structure of the beam is observed in this plane. Figure 13(a) and 13(b) are the beams in the Arms 1 and 2 respectively, and Fig. 13(c) is the radially polarized superposition beam.

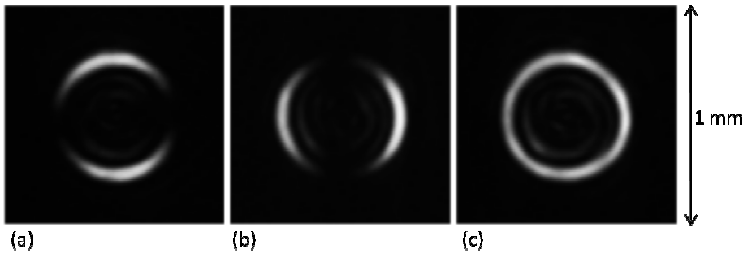

Fig. 13. FIP intensity distributions of the beams transmitted via Arm 1 (a), Arm 2 (b) and the radially polarized superposition beam obtained using method 1 and the imaging system shown in Fig. 12.

4. Conclusions

We have demonstrated theoretically and experimentally two related methods of using ICD for the conversion of a linearly polarized Gaussian laser beam to a beam with radial polarization. In the near-field of the radially polarized beam, which corresponds to the FIP in ICD, the beam profile can be adjusted from a sharp double ring profile for high ρ_0 to one that closely matches a Laguerre-Gaussian for low ρ_0, while in the far-field the profile approaches that of a first order Bessel beam for high ρ_0. Both of these beam profiles are readily accessible by simple adjustment of the experimental setup. Apart from the usual reflection losses at optical interfaces, the technique is highly efficient. Taking a linearly polarized input beam, the

#152718 - $15.00 USD Received 10 Aug 2011; revised 21 Sep 2011; accepted 21 Sep 2011; published 20 Oct 2011

efficiency of Method 1 is 50% for the high ρ_0 used here and that of Method 2 is 100%. The efficiency of Method 1 can be even higher for ICD with lower values ρ_0 since in that case the B_1 component carries a larger fraction of the optical power [19]. The very high optical quality of currently available biaxial crystals ensures the fidelity of the radially polarized beams is very high. The biaxial crystal is highly transparent in the visible spectral region, thus the technique can be considered for high power applications of radially polarized beams.

Acknowledgments

We wish to acknowledge the support of Science Foundation Ireland under research grant 08/IN.1/I1862.

#152718 - $15.00 USD Received 10 Aug 2011; revised 21 Sep 2011; accepted 21 Sep 2011; published 20 Oct 2011